Decisions Made with Less Evidence Involve Higher Levels of Corticosubthalamic Nucleus Theta Band Synchrony

Baltazar Zavala[1,2], Huiling Tan[1,3], Simon Little[4], Keyoumars Ashkan[5], Alexander L. Green[1,3], Tipu Aziz[1,3], Thomas Foltynie[4], Ludvic Zrinzo[4], Kareem Zaghloul[2], and Peter Brown[1,3]

Abstract

■ The switch between automatic action selection and more controlled forms of decision-making is a dynamic process thought to involve both cortical and subcortical structures. During sensory conflict, medial pFC oscillations in the theta band (<8 Hz) drive those of the subthalamic nucleus (STN), and this is thought to increase the threshold of evidence needed for one competing response to be selected over another. Here, we were interested in testing whether STN activity is also altered by the rate at which evidence is presented during a congruent dot motion task absent of any explicit sensory conflict. By having a series of randomly moving dots gradually transform to congruent motion at three different rates (slow, medium, fast), we were able to show that a slower rate increased the time it took participants to make a response but did not alter the total amount of evidence that was integrated before the response. Notably, this resulted in a decision being made with a lower amount of instantaneous evidence during the slow and medium trials. Consistent with the idea that medial pFC–STN activity is involved in executing cognitive control, the higher levels of ambiguity during these trials were associated with increased theta band synchrony between the cortex and the STN, with the cortical oscillations Granger-causal to those of the STN. These results further confirm the involvement of the STN in decision-making and suggest that the disruption of this network may underlie some of the unwanted cognitive deficits associated with STN deep brain stimulation. ■

INTRODUCTION

Throughout each day, we make hundreds of decisions that vary in their level of difficulty. Some decisions can be very easy (should I wear sneakers or dress shoes for my big presentation), some can be moderately challenging (should I take the short route to work or the route with less traffic), and some can be very difficult (should I switch careers). The neuronal mechanisms responsible for determining what actions we choose and when we choose to execute them are complex and have received much attention in the field of neuroscience. This work has led to various computational models that attempt to explain how we dynamically adjust the resources allocated for a decision based on the difficulty of that decision. One of these models, known as the drift diffusion model, posits that when an individual must choose between two competing alternatives, noisy neuronal processes accumulate information supporting each of two alternatives until the difference in neurophysiological evidence is high enough to cross a decision boundary and execute the winning response (Ratcliff & McKoon, 2008). According to this model, the timing of a decision can be affected in part by the rate at which evidence is accumulated (the drift rate) and the amount of evidence that is required for one alternative to beat the other (the evidence threshold).

Over the past few years, there has been a growing body of work suggesting that one area of the brain that is involved in the dynamic adjustment of the evidence threshold during high conflict scenarios is the subthalamic nucleus (STN). According to the models that initially predicted the STN's involvement (Bogacz & Gurney, 2007; Frank, 2006), when two conflicting motor commands are simultaneously activated, the activation of the STN via hyperdirect cortical inputs results in elevated BG firing and thus an increased inhibition of the thalamus. In line with these predictions, it has been subsequently shown that disruption of the STN via high-frequency deep brain stimulation (DBS) for Parkinson disease (PD) results in an impaired ability to adjust the evidence threshold during conflict (Green et al., 2013; Cavanagh et al., 2011), which leads to impulsive, incorrect responses in the laboratory setting (Antoniades et al., 2014; Coulthard et al., 2012; Frank, Samanta, Moustafa, & Sherman, 2007). Further support for the claim that the STN is involved in dynamically adjusting the response threshold stems from the fact that PD patients who have received DBS to the STN

[1]University of Oxford John Radcliffe Hospital, [2]National Institutes of Health, Bethesda, MD, USA, [3]Medical Research Council Brain Network Dynamics Unit at the University of Oxford, [4]University College London, [5]Kings College, London, UK

Journal of Cognitive Neuroscience 28:6, pp. 811–825
doi:10.1162/jocn_a_00934

self-reported higher impulsivity scores than non-DBS PD patients when evaluating their day-to-day lives (Hälbig et al., 2009, but see also Zavala, Zaghloul, & Brown, 2015). As of yet, however, it remains unclear what mechanisms are responsible for triggering the STN's posited "hold your horses" function and what scenarios result in their activation.

Recently, it has been suggested that one mechanism by which the STN could be informed for the need to adjust the evidence threshold during conflict is by rapid, frequency-specific activation by the medial pFC (mPFC). Previous studies have demonstrated that tasks involving high levels of conflict are associated with increased 4–8 Hz theta band activity in the mPFC and that this activity correlates with variations in RT (Cohen & van Gaal, 2014; Cavanagh, Zambrano-Vazquez, & Allen, 2012; Cavanagh et al., 2011; Cohen & Cavanagh, 2011). Given that areas within the mPFC, such as the ACC (Cavanagh & Shackman, 2015; White, Engen, Sørensen, Overgaard, & Shergill, 2014; Mushtaq, Bland, & Schaefer, 2011; Stern, Gonzalez, Welsh, & Taylor, 2010; Krain, Wilson, Arbuckle, Castellanos, & Milham, 2006; Botvinick, Cohen, & Carter, 2004), are thought to be crucial for detecting situations requiring cognitive control, the elevated theta band activity is thought to be generated by these structures (Womelsdorf, Johnston, Vinck, & Everling, 2010; Womelsdorf, Vinck, Leung, & Everling, 2010; Tsujimoto, Shimazu, & Isomura, 2006; Wang, Ulbert, Schomer, Marinkovic, & Halgren, 2005; Gevins, Smith, McEvoy, & Yu, 1997) as a way of recruiting downstream targets necessary for implementing such control (Cavanagh et al., 2011, 2012). In line with this hypothesis, our previous study involving a dot motion discrimination task showed that theta band activity in the STN became synchronized to that in the mPFC, but only when two populations of dots were moving in conflicting directions (Zavala et al., 2014). Finally, it has been shown that disruption of the STN via DBS also disrupts the relationship between mPFC theta band activity and adjustments to the decision threshold based on conflict (Cavanagh et al., 2011).

Although the work mentioned above together suggests that the STN is indeed involved in adjusting the evidence threshold during conflict, here we were interested in testing whether the synchronization between mesial frontal cortex and STN buys time when deciding what to do and precisely when to do it is difficult, regardless of whether this is due to the simultaneous activation of conflicting actions or due to sensory uncertainty. To test this, we designed a paradigm in which a group of randomly moving dots gradually became coherent in one direction, but the rate at which they became coherent was set to three different speeds (slow, medium, and fast). Our paradigm revealed that, prior to a decision, participants integrated the amount of instantaneous dot congruency over time until an equal amount of integrated evidence had been reached for the three different conditions. Notably, this resulted in a decision being made with a lower level of instantaneous dot congruency at the time of the response for the slow and medium trials. Crucially, the theta band synchrony between the STN and cortical EEG electrodes became elevated during the slow and medium trials, possibly reflecting the increased need for cognitive control due to the lower levels of dot congruency leading up to the response. These results lend support to the hypothesis that cortical STN synchrony plays a role in delaying an action when there is uncertainty in what the correct response should be, even when this might arise through sensory uncertainty rather than explicit conflict between competing possible actions.

METHODS

Participants and Task

Sixteen participants (10 men, mean disease duration = 11 years, mean age = 55 years, range = 38–66 years) underwent bilateral implantation of DBS electrodes into the STN, as a prelude to high-frequency stimulation for the treatment of advanced PD. Thirteen of these participants also performed another dot motion discrimination task, the results of which have been reported (Zavala et al., 2014). Techniques to target and implant electrodes in the STN have been described (Foltynie & Hariz, 2010). At University College London Hospital, patients were operated on under general anesthesia, and lead location was confirmed with intraoperative stereotactic MRI. At the John Radcliffe Hospital and King's College Hospital, where implantation was performed with patients awake, effective stimulation was confirmed intraoperatively, and lead location was further confirmed with immediate postoperative stereotactic computerized tomography. The permanent quadripolar electrode used was model 3389 (Medtronic Neurologic Division, Minneapolis, MN) featuring four platinum–iridium cylindrical surfaces. Electrode extension cables were externalized through the scalp to enable recordings prior to connection to a subcutaneous DBS pacemaker, implanted in a second operation up to 7 days later.

Patients participated in a decision-making task while on their regular medication 3–6 days after electrode implantation. All participants gave their written informed consent to take part in the study, which was approved by the appropriate local ethical committees. Clinical details of the patients are provided in Table 1. The mean percentage improvement in the motor section of the Unified Parkinson Disease Rating Scale (UPDRS) on treatment with levodopa was 63 ± 3% across participants ($p < .0001$, paired t test between ON and OFF levodopa scores for the 15 participants with UPDRS scores: Case 4's scores were unavailable). Cases 13 and 16 had been diagnosed as having an impulse control disorder. However, neither showed task performance or electrophysiological behavior that deviated significantly from that of the remaining participants during the paradigm. In

Table 1. Clinical Details

Case	*Age*	*Disease Duration*	*UPDRS Off (III)*	*UPDRS On (III)*	*First Symptom*	*Reasons for Surgery*	*Daily Medication (mg/day)*	*Hospital*
1	62	29	57	17	Impaired mobility	Bradykinesia, Motor fluctuations	Levodopa 650; Amantadine 200; Selegiline 5; Ropinerole 8	UCL
2	49	10	42	6	Tremor	Tremor	Levodopa 300; Trihexyphenidyl 2	OX
3	50	9	58	23	Shoulder stiffness	Motor fluctuations, tremor	Levodopa 1050	KC
4	50	4	N/A	N/A	Right arm tremor	Tremor	Levodopa 400; Rotigotine 16; Entacapone 600	KC
5	66	16	32	13	Loss of dexterity	Bradykinesia	Levodopa 600; Amantadine 200; Ropinerole 24; Rasagiline 1	UCL
6	51	7	58	13	Loss sense of smell	Tremor, gait difficulties	Levodopa 1300	UCL
7	64	12	70	20	Tremor	Dyskinesias	Levodopa 1200; Apomorphine 7 mg/hr	UCL
8	47	14	34	11	Left arm bradykinesia	Dyskinesias, motor fluctuations	Levodopa 350; Pramipexole 1.05; Amantadine 300	UCL
9	66	14	63	24	Shoulder pain & stiffness	Motor fluctuations	Levodopa 650; Pergolide 9	UCL
10	38	10	69	30	Right arm tremor	Tremor, bradykinesia	Apomorphine 10; Levodopa 600–800	KC
11	62	2.5	18	8	Left side tremor	Tremor, rigidity	Levodopa 800	OX
12	57	7	43	17	Left hand tremor	Tremor	Levodopa 600; Rotigotine 8; Ropinerole 8; Rasagiline 1; Entacapone 1200	UCL
13	57	6	21	7	Left side bradykinesia	Dyskinesias, motor fluctuations	Levodopa 750; Entacapone 1000	UCL
14	61	4	37	15	Left side tremor	Tremor	Amantadine 200; Levodopa 750; Entacapone 1000	KC
15	65	15	51	21	Left hand tremor	Freezing	Amantadine 200; Levodopa 400; Ropinirole 12	UCL
16	42	9	60	42	Loss of dexterity	Bradykinesia, dystonia	Amantadine 400; Levodopa 600	UCL

UPDRS = Part III motor score of the United Parkinson Disease Rating Scale.

particular, the mean RTs for the two patients with impulse control disorders were 2.840 and 2.366 sec, which fell well within the range of the other 11 patients (1.689–4.688 sec).

A schematic of the task is shown in Figure 1A. Participants were asked to stare at a target circle containing 200 randomly moving white dots presented on a black background. The task was generated using the program Psychopy (Peirce,

2007) and presented on a 33-cm Macintosh laptop (60 Hz screen refresh rate). The target circle was 14 cm in diameter, and the white dots were 10 pixels large (visual angle ≈ 0.25°). Before the beginning of the experiment, the participants were asked to indicate the overall direction the dots were moving whenever they noticed that the dots were congruently moving either left or right. Left direction choices were indicated with a left index finger press of the "z" key on the keyboard, and right direction choices were indicated with a right index finger press of the "/" key. Each randomly moving dot moved in a straight line at a rate of 0.14 mm per frame for 20 frames (333 msec) before moving to another part of the target circle and moving in a new direction chosen pseudorandomly between −180° and 180°. This was done to prevent the participants from focusing on any individual dot and using it to identify the congruent motion of the dots.

Three types of trials were randomly shown throughout the experiment. One third of the trials (28 of 84 trials) were what we will refer to as "fast trials." At the beginning of all fast trials, some of the dots started moving horizontally to either the right (0°) or the left (180°) of the screen. The number of dots moving congruently in one direction increased linearly from 0% to 50% at a rate of 0.004% per frame. By 2.083 sec, the maximum number of dots moving congruently during the fast trials had been reached (100 dots, i.e., 50% of all 200 dots). The second and third groups of trials (28 trials each) were what we will refer to as "medium trials" and "slow trials", respectively. These trials were identical to the fast trials with the exception that the rate at which the dots became increasingly congruent was 0.002% per frame for the medium trials and 0.001% per frame for the slow trials. By 4.17 and 8.333 sec, the maximum number of dots (again 100)

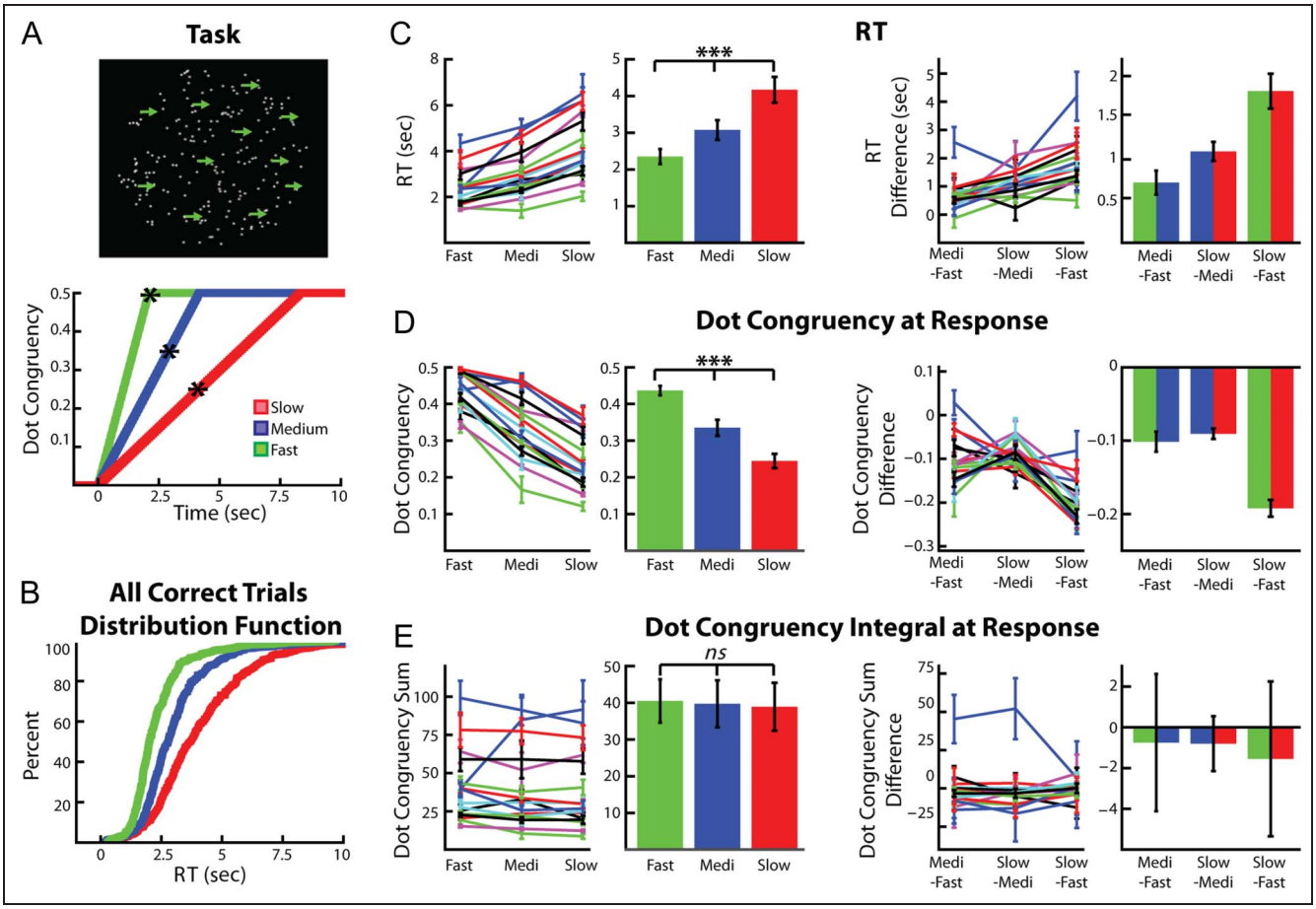

Figure 1. Task and behavior. (A, top) Randomly moving dots were displayed continuously on screen. During all trials, dots began moving coherently in one horizontal direction until either 50% of the dots moved coherently, the participant indicated the direction he or she perceived the dots were moving in, or the trial timed out after 14 sec. (A, bottom) Three trial types were used, with the only difference between trials being the rate at which the dots became increasingly congruent. Asterisk denotes average RT for each trial type. (B) Cumulative distribution function (CDF) of the RTs for all of the fast (green), medium (blue), and slow (red) trials (collapsed across all participants) used in the analysis. (C) Mean RTs for the three conditions were significantly different. Left two panels show each trial type's average RT for each participant (mean ± *SEM*) as well as the average RT across participants (mean ± *SEM*). Right two panels show the difference between trial types for each participant (mean ± standard error of the difference, SED) and the average across participant difference (mean ± *SEM*). (D) On average, participants responded with a lower instantaneous dot congruency (and thus a higher level of stimulus ambiguity) in the slow trials, followed by the medium trials and then the fast trials. Format as in C. (E) The integral of instantaneous dot congruency (from congruent motion onset until the response) was equal for all three conditions. Format as in C. ***$p < .0001$.

moving congruently during the medium and slow trials, respectively, had been reached. Regardless of trial type, participants were instructed to indicate the direction of the majority of the dots. If the participant answered incorrectly or took longer than 14 sec to indicate a response, the word "incorrect" was briefly displayed in the center of the screen for 0.75 sec. Incorrect trials were excluded from all analysis. Participants were allowed to practice the task as long as they wished before the electrophysiological recordings were made. The practice sessions were generally quite short (<10 trials), as the task was designed to be as simple as possible.

It is important to note here that at no point were the participants given a "cue" indicating that a trial had begun. In other words, there was never a defined stimulus onset, and all increases in congruent dot movement were gradual. After the participant pressed a keyboard key to indicate his or her response for a given trial, all dots immediately began to move in random directions. They continued to do so for a pseudorandomly chosen time period of no less than 2 sec and no more than 4 sec before slowly starting to move congruently again for the next trial. Only when the participant noticed that the dots were moving congruently to the left or the right did the participant become aware that the trial had begun. These gradual changes were designed to suppress neuronal activity caused by abrupt stimulus changes and to increase the separation in time of neuronal activity associated with uncertainty from neuronal activity associated with motor processing or movement (Zavala et al., 2014; O'Connell, Dockree, & Kelly, 2012). Nevertheless, for simplicity we will refer to the time point at which the dots began moving congruently as the "trial onset." Before the "trial onset," there was a period of 2–4 sec during which all dots were moving in random directions. For the comparison of correct fast, medium, and slow trials, all incorrect responses (13.7 ± 2.3% of all trials) were discarded. A one-way repeated-measures ANOVA was used to evaluate whether the participant's mean RTs or error rates were significantly different between the three trial types.

Electrophysiological Data Recording

STN local field potentials (LFPs) were recorded from the DBS electrodes. Simultaneously, continuous scalp EEG was recorded from frontocentral, central, and parietal electrodes at the midline (FCz, Cz, and Pz, International 10–20 System). More lateral electrodes were prohibited by surgical wounds and dressings in this patient group. All signals were sampled at 2048 Hz, band-pass filtered between 0.5 and 500 Hz, and amplified using a TMSi porti amplifier and its respective software (TMS International, Oldenzaal, Netherlands). Data were analyzed using custom written Matlab (The MathWorks, Inc., Natick, MA) scripts. Before any analysis, monopolar recordings were down-sampled to 1000 Hz, notch-filtered at 50 Hz, and converted to a bipolar montage between contacts (three bipolar channels per STN side and two bipolar channels for the EEG recordings: FCz-Cz and Pz-Cz). Rereferencing was done so as to limit the effects of volume conduction from distant sources. The data were then epoched into 5-sec long runs beginning 1 sec before the onset of progressive dot motion congruency (henceforth referred to as trial onset) for the trial onset aligned data and beginning 4 sec before the response for response aligned data. An additional buffer of 1 sec was also included on either side of each epoch, but this buffer was discarded after the extraction of power, phase, or connectivity measures. Any trial with a clear artifact in either the EEG or LFP bipolar traces was discarded (mean final trial count after removing artifact trials and incorrect response trials = 72.0 ± 4.8 trials per participant). For two participants (Case 3 and Case 12), the entire recording had to be discarded due to artifacts, and therefore, the total number of participants included in the electrophysiological analysis was 14.

Induced Power and Phase Consistency Analysis

To analyze changes in induced power during the task, the following approach was applied separately to each of the three types of trials (fast, medium, slow) as well as to the average of all correct trials. First, the mean ERP in each of the three STN bipolar recordings and both of the EEG bipolar recordings was calculated by averaging the raw bipolar signal across trials. The ERP was then subtracted from each trial's raw time series to isolate the non-phase-locked activity in the signal. The power of the resulting signal was then calculated using the Morlet wavelet at 8 scales/octave from 2 to 107 Hz, and the resulting power matrices were averaged across trials. This method produced a time–frequency image for fast, medium, and slow trials for each of the three bipolar contacts on each STN electrode and each of the two EEG bipolar contacts. Each channel's time–frequency pixels were then normalized to that channel's mean power in that frequency recorded during a "baseline" period of all trials. The baseline was chosen to be a 1-sec long time period between trials during which all dots moved randomly in any direction. The normalized induced power was then averaged across the three bipolar contacts in each STN and then across each participant's two STNs. Averaging across all the contact pairs in a given participant was performed so as to avoid selection bias, although this procedure might serve to underestimate spectral changes in the STN as not all contact pairs were necessarily within or bridging this nucleus. In two of the STNs, only one bipolar channel was available because one of the electrode's middle two contacts did not record usable LFP activity. Furthermore, two participants (Case 2 and Case 11) were only implanted in one STN, so the final across STN average step was omitted for these participants.

To assess the statistical significance of the mean induced power difference between any two trial types

(i.e., fast vs. slow trials), the mean difference across all 14 participants was found between the two conditions, and the same procedure was repeated 1000 times with the fast and slow (or medium) labels of each participant's average data randomly assigned during each permutation (Maris & Oostenveld, 2007). The p value of each time point was found by comparing the actual mean difference to the distribution of the 1000 permutations for that time point. This same procedure was also used to determine when power levels significantly differed from baseline, but in this case each participant's average normalized power across all trials was permuted with an equally sized time-by-frequency matrix of zeros. This allowed us to identify contiguous time–frequency points that were significantly different from zero.

Following any permutation procedure, the resulting p values were then corrected for multiple comparisons using exceedance mass testing (Maris & Oostenveld, 2007). Exceedance mass testing involves integrating the excess mass of suprathreshold clusters in the time-by-frequency matrix and recording the largest per iteration. For each cluster that was larger than 95% of the distribution, a p value is reported. Throughout all of our analyses, exceedance mass testing was used to correct for multiple comparisons whenever the difference in a continuous time–frequency spectrogram or a continuous time series between two conditions was assessed. This allowed us to take into account when adjacent points were significant, whereas more traditional methods of correction such as Bonferroni or false discovery rate assume that all time points are independent measurements. When only individual, noncontinuous values were compared between trial types, more traditional parametric statistics (i.e., t tests and ANOVAs) were used.

To analyze the phase consistency across trials, the phase of the bipolar channels was calculated using the Morlet wavelet at 8 scales/octave from 2 to 107 Hz. For this analysis, the raw bipolar signal (not the ERP subtracted signal used for the induced power calculation) was used. The intertrial phase consistency (ITPC, sometimes also called intertrial phase clustering; Cohen & Gulbinaite, 2014) was then found at each time–frequency point by projecting the phase at time t for each trial onto the complex plane, averaging across trials, and taking the absolute value. Using this formulation, an ITPC(t) value of 0 would mean there is a uniform distribution of phase across trials at time t for a specific frequency, and a value of 1 would mean that the phase at time t is identical for that frequency for each trial. ITPC values were calculated separately for fast, medium, and slow trials. To prevent any differences in trial count from affecting our results, two of the trial types were subsampled for each participant in such a way that the number of trials in each trial group matched the trial group with the fewest trials. One thousand subsampled ITPC spectrograms were calculated for each participant, and the average of the subsampled–sampled values was used. All three trial types were then normalized to the ITPC value recorded during the "baseline" period defined above. Randomly drawn subsets of all the trials were used to calculate the baseline 1000 times, with the number of trials used for each baseline calculation equal to the number of trials in the trial group with the fewest trials (and the number of subsampled trials in the other two groups). Qualitatively very similar results were obtained if the trial counts were not subsampled to match each other, which is consistent with the fact that the trial counts were very similar across conditions (mean trial counts = 24.4 ± 1.5, 23.8 ± 1.8, and 23.8 ± 1.6 for fast, medium, and slow trials, respectively).

To assess the statistical differences between two conditions, the two normalized ITPCs were first calculated for each bipolar signal and averaged across all bipolar contact pairs of each STN electrode and then across STN electrodes. The difference between the two conditions was then found before being averaged across all 14 participants. Time–frequency points exhibiting significant differences between conditions or significant changes from baseline were then found using the permutation procedure described above, with the only difference being that the ITPC values were used instead of the induced power values.

Intersite Coherence

The cortex–STN coherence was calculated using the continuous time evolving methods we have previously used (Zavala et al., 2014) as outlined by Lachaux et al. (2002). As in our previous work, we use the term coherence to refer to the correlation coefficient of two signals in the frequency domain (Pesaran, 2008; Lachaux et al., 2002; Gardner, 1992). Coherence is essentially an estimate of the consistency of the phase difference between the two signals and the correlation of the two signal's power. It is estimated by calculating the average cross-spectrum of the two signals and dividing by the product of each signal's autospectrum.

Fast, medium, and slow trials were analyzed separately, with the coherence values being calculated 1000 times using a subsampled data set in which the trial count was equal for all three trial types (see ITPC section above). As in the ITPC analysis, the raw signal at each bipolar contact was convolved with the Morlet wavelet to generate a complex value for each time–frequency point. The cross-spectrum at each time–frequency point was then found by multiplying the LFP's complex wavelet value at each point in each trial by the conjugate of the EEG's complex wavelet value for the corresponding time–frequency point. The complex cross-spectrum values were then averaged across trials, and a sliding window was used to integrate across time (Lachaux et al., 2002). The width of the temporal integration window was varied according to the frequency being analyzed. On the basis of the recommendations made by Lachaux et al. (2002), the width was

chosen to be 8 cycles of each oscillatory frequency (i.e., 8 cycles at 4 Hz = 2000 msec, 8 cycles at 8 Hz = 1000 msec, 8 cycles at 16 Hz = 500 msec, etc.). The absolute value of the resulting average cross-spectrum was then divided by the product of the two signal's autospectra to generate the wavelet coherence. Each channel's time evolving coherence signal was then normalized by that channel's "baseline" coherence at each frequency. The baseline was chosen in the same way as it was for the ITPC analysis: calculating the mean coherence value (averaged across the "baseline" period defined above) 1000 times for subsampled sets of trials (equal in number to the trial count of the smallest group of trials) randomly chosen from all of the trials. The theta coherence time series were produced by averaging the coherence values between 4 and 8 Hz for each trial type.

The statistical differences between pairs of conditions were assessed in the same way as for the ITPC. Cortex–STN coherence was separately estimated for the Pz-Cz and FCz-Cz bipolar electrodes. As a final validation of our results, the same analysis outlined above for the wavelet coherence was redone using only the phase values, that is, the phase coherence or intersite phase clustering (Cohen & Gulbinaite, 2014). In other words, instead of finding the magnitude of the average cross-spectrum and dividing by the average autospectrum at each time point, the magnitude of the average phase difference between the LFP and the EEG signals was calculated at each time point. This method produced qualitatively very similar results (data not shown) as those obtained for the wavelet coherence measurement (Figure 4).

Granger Causality Analysis

We used multivariate autoregressive (MVAR) modeling to estimate the spectral Granger causality (Seth, 2010; Ding, Chen, & Bressler, 2006; Kamiński & Blinowska, 1991; Granger, 1969) between LFP signals recorded from the STN and EEG signals recorded over the frontal and posterior cortices. When we say that one signal is "Granger-causal" to a second signal, we mean that the inclusion of past observations of the first signal reduce the prediction error of the second signal in a linear regression model (relative to a model that only includes past observations of the second signal; Seth, 2010; Granger, 1969). To preprocess the data and calculate the MVAR estimated Granger causality, the Granger causality connectivity analysis toolbox (Seth, 2010) was used to analyze the raw, bipolar EEG and LFP signals.

Before any analysis, 50-Hz mains artifact was removed by notch filtering, and the data were downsampled to 200 Hz. This was done so as to improve frequency resolution while maintaining the timescale of the interactions (Ruiz et al., 2014; Schlögl & Supp, 2006). Because our recordings took place over multiple trial iterations (as opposed to one long recording), each trial was treated as an independent realization of a statistically stationary process. To minimize nonstationarities across trials, each bipolar channel was normalized horizontally and vertically as follows (Seth, 2010; Ding, Bressler, Yang, & Liang, 2000). First, each trial was zero-meaned across time (horizontal normalization) by subtracting the mean voltage amplitude of that trial from each time point in the trial and dividing the resulting values by the standard deviation of the voltage amplitude of that trial (Ding et al., 2000). Next, the mean and standard deviation of the evoked response (averaged across all trials) was calculated, and each corresponding time point in each trial was z-scored (vertical normalization) by the appropriate values corresponding to that time point in the evoked response (Seth, 2010; Ding et al., 2000). The vertical normalization step was done separately for each trial group. Although vertical normalization is consistently used in the literature (Ruiz et al., 2014; Brovelli et al., 2004) to "(1) remove the first-order nonstationarity from the data and (2) make the ensemble mean equal to zero" (Ding et al., 2000), we found qualitatively very similar results when the vertical normalization step was omitted (data not shown). This is most likely due to our use of gradual changes in the dot coherence that never resulted in a stimulus onset-triggered evoked response. After the data were preprocessed, each 5-sec trial was windowed into 1500-msec windows spaced every 250 msec (21 windows total). The spectral Granger causality (Seth, 2010) between each LFP–EEG bipolar pair was then found by calculating the MVAR model matrix for each trial, averaging the MVAR matrixes across trials and converting the matrix into the spectral domain using the "cca_pwcausal" function of the Granger causality connectivity analysis toolbox (Seth, 2010; Ding et al., 2000; Kamiński & Blinowska, 1991; Geweke, 1982). The model order used in our analysis (i.e., the number of time lags to include when generating the MVAR model matrix) was chosen to be 25. Given our 200-Hz sampling rate, our model order of 25 steps corresponds to "looking into the past" for 125 msec, which is long enough to resolve frequencies in the theta band (Cohen, 2014). The three different trial types were analyzed separately for each electrode pair and then normalized using the same baseline value. The baseline was found by calculating the mean spectral Granger causality during the "baseline" period for all three trial types and averaging across the three trial types. The theta band time series were produced by averaging the spectral Granger causality values between 4 and 8 Hz for each trial type. Once the LFP–EEG theta Granger causality had been normalized for each of the three bipolar contacts, it was averaged across contacts and then across STNs, giving a mean STN–EEG spectrogram for each participant. The mean difference across all participants was then found, and this mean difference was compared with 1000 permuted differences found by randomly permuting the labels of each participants's average data before averaging across participants. To correct for multiple comparisons across time points, exceedance mass testing was used as detailed above (Maris & Oostenveld,

2007). This entire procedure was done separately for the EEG–STN spectral Granger causality and the STN–EEG spectral Granger causality.

RESULTS

Task and Behavior

Sixteen patients receiving DBS implantation surgery for PD performed the task shown in Figure 1. At the beginning of each trial, dots that were randomly moving in all directions of the screen gradually and, without warning, increased their congruent horizontal motion to either the left or the right. Three trial types were used, fast, medium, and slow, with the only difference between trials being the rate at which the dot motion congruency was increased linearly over time. The task used was similar to that previously reported by us (Zavala et al., 2014), in so far as all changes in dot motion congruency were gradual and at no point were participants informed that a trial had commenced (i.e., there was no cue). However, there was one critical difference with respect to the previous task; none of the trials in the current study involved explicit sensory "conflict," and only the rate at which information was presented was altered.

On average, participants required 2.35 ± 0.20 sec (mean ± *SEM*) to respond on fast trials, 3.07 ± 0.27 sec to respond on medium trials, and 4.17 ± 0.35 sec to respond on slow trials (Figure 1C). A repeated-measures one-way ANOVA revealed a very significant difference in RT between the three conditions ($F = 65.14$, $df = 2$, $p < .0001$). Post hoc t tests revealed that the medium trial RTs were significantly slower than the fast trial RTs ($p < .001$) and the slow trial RTs were significantly slower than both the medium and fast trials ($p < .0001$ for both). An across-subject repeated-measures one-way ANOVA did not reveal any significant differences in error rate across the three conditions ($F = 1.29$, $df = 2$, $p = .29$).

Figure 1D shows the average dot motion congruency at the time of the response for the three different conditions. This reveals that, at the time of the response, participants made their decisions with a lower dot motion congruency (i.e., less information) during slow trials (average dot motion congruency = 24.0 ± 1.9%) than they did during medium (33.1 ± 2.2%) and fast (43.6 ± 1.3%) trials (ANOVA, within-subject repeated-measures, $F = 150.9$, $df = 2$, $p < .0001$). In contrast, the integral of the dot motion congruency (from the onset of progressive dot motion congruency until the response) was not different across the three conditions (ANOVA, within-subject repeated-measures, $F = 0.13$, $df = 2$, $p > .88$). This suggests that, although evidence was presented to the participants at a slower rate during the slow and medium trials, the longer time period of evidence integration during these trials allowed the participants to ultimately respond with a lower degree of instantaneous dot motion congruency then they did during the fast trials. The result of this, however, was that the medium and slow trial responses were made when the ambiguity in the stimulus was higher than that experienced at the time of response for the fast trials.

To confirm that the differences in instantaneous dot congruency at the time of the response were not due to the more rapid dot congruency increases during any "nondecision time" in between when the participants made their decision and when they executed their response, we also calculated the average dot congruency 500 msec before the participants made their response. These values were 36.3 ± 2.1%, 28.4 ± 2.4%, and 21.6 ± 1.2% for fast, medium, and slow trials (ANOVA, within-subject repeated-measures, $F = 88.9$, $df = 2$, $p < .0001$), respectively. This suggests that the differences were not due to dot congruency increases after the decision was made (but before the response was executed) and that the participants did indeed make their decision with less instantaneous "evidence" during the slow and medium trials relative to the fast trials. This assumes a nondecision time of 500 msec, which is much longer than that typically assumed in the literature (Ratcliff & Frank, 2012; Ratcliff & McKoon, 2008; Ratcliff & Tuerlinckx, 2002). Similarly significant results were also observed if we assumed a nondecision time of 1 sec (ANOVA, within-subject repeated-measures, $F = 23.4$, $df = 2$, $p < .0001$).

Power and ITPC Changes during the Task

Figure 2 shows the average changes in power that occurred during the task for the STN and for two midline EEG cortical recordings in the frontal (FCz-Cz) and parietal cortex (Pz-Cz). Although the spectrograms suggest an increase in STN theta and delta band activity during the task, only the response-aligned decreases in beta band activity survived correction for multiple comparisons ($p = .008$, permutation testing). Similarly, in the frontal and parietal cortex, only the cue and response aligned beta changes were significantly different from baseline ($p < .001$, permutation testing). These significant changes from baseline were observed when all trials were averaged together, but no significant trial type-related differences in power were observed during the task ($p > .05$, permutation testing). ITPC was also analyzed during the task, and this revealed a significant increase in delta band ITPC at the time of the response for the STN and the midline frontal cortex recordings (Figure 3). Once again, however, there were no trial type-related differences in ITPC during the task ($p > .05$, permutation testing).

Frontal EEG–STN Synchrony Changes during the Task

Despite not showing any trial type-related differences in theta power or ITPC, our data revealed significant, trial type-related differences in the level of theta band synchrony

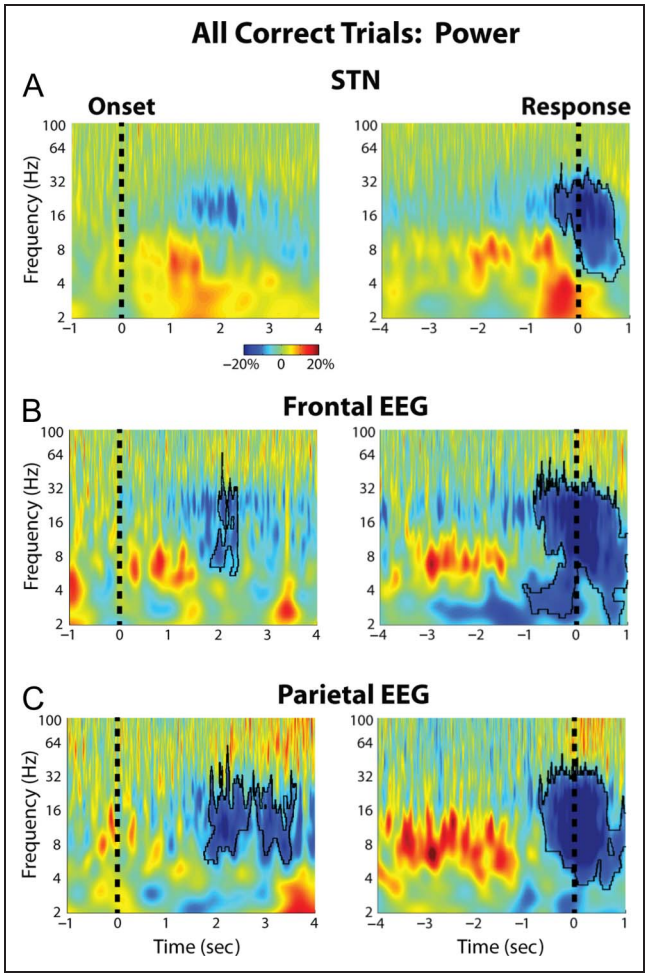

Figure 2. Group average percentage power changes in STN LFP and cortical EEG. (A) STN LFP power changes aligned to the congruent dot motion onset (left) and to the response (right). Black outline denotes time–frequency clusters determined to be significantly different from baseline ($p = .008$, permutation testing). The baseline was chosen to be a 1-sec long time period between trials during which all dots moved randomly in any direction. (B) Same as A but for the FCz-Cz frontal cortical electrode ($p = .011$, for the cue aligned data and $p = .001$ for the response aligned data, permutation testing). (C) Same as A but for the Pz-Cz parietal cortical electrode ($p = .017$, for the cue aligned data and $p = .001$ for the response aligned data, permutation testing). There were no significant differences in induced power between the different trial types.

between the medial frontal EEG and the STN. Spectrograms of the wavelet coherence aligned to the onset of progressive dot motion congruency for all three conditions are shown in Figure 4A (left). These plots revealed that during the slow and medium trials, there was an increase in (FCz-Cz)–STN theta coherence that was significantly greater than that observed during the fast trials ($p = .023$ and $p = .031$ for the slow vs. fast and medium vs. fast comparisons, respectively, permutation testing; Figure 4A, right). Comparing the theta coherence time series (Figure 4A, bottom right) also revealed these differences ($p = .003$ and $p = .004$ for the slow vs. fast and medium vs. fast comparisons, respectively, permutation testing) and further showed that the slow trial coherence remained elevated longer than the medium trial coherence. Although this is consistent with the longer RTs of the slow trials, it is unlikely that these differences were due to a time on task effect in which theta coherence continues to rise throughout the trial (Cohen & Nigbur, 2013; Scherbaum & Dshemuchadse, 2013; Zavala et al., 2013; Nachev, 2011; Yeung, Cohen, & Botvinick, 2011); in the response aligned version of these plots (Figure 4B) coherence between the STN and the frontal cortex increased to similar levels in both the medium and slow trials, despite an RT difference (and thus a difference in time spent on task) of approximately 1 sec. The response-aligned data revealed that roughly 1.5 sec before the response, the theta coherence during the slow and

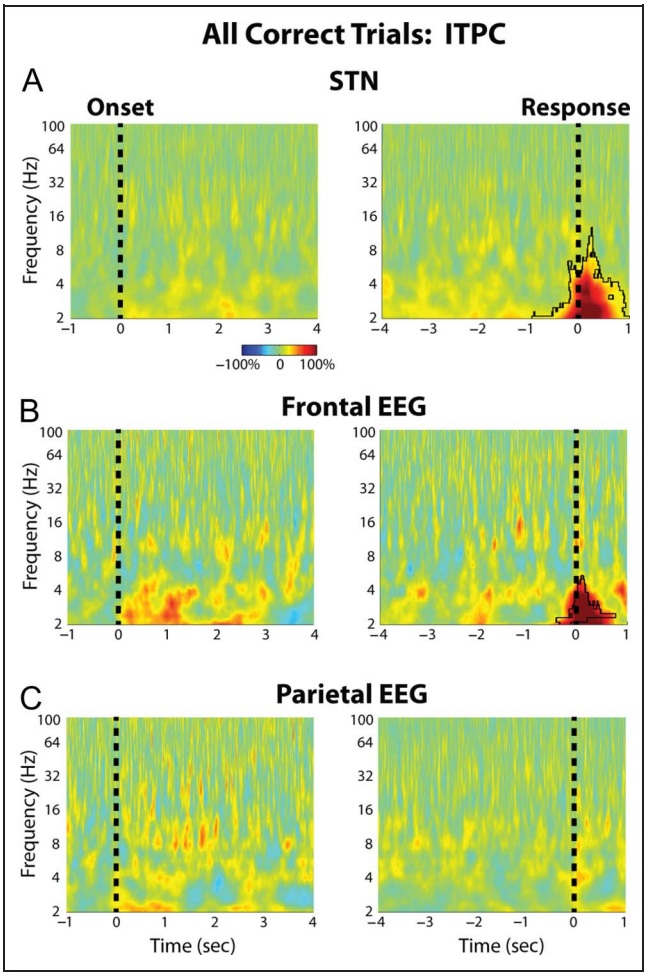

Figure 3. Group average percentage chance in STN LFP and cortical EEG ITPC. (A) STN LFP ITPC changes averaged across all three trials are shown aligned to the congruent dot motion onset (left) and to the response (right). Black outline denotes time–frequency clusters determined to be significantly different from baseline ($p = .001$, permutation testing). The baseline was chosen to be a 1-sec long time period between trials during which all dots moved randomly in any direction. (B) Same as A but for the FCz-Cz frontal cortical electrode ($p = .006$, for the response aligned data, permutation testing). (C) Same as A but for the Pz-Cz parietal cortical electrode. There were no significant differences in ITPC between the different trial types.

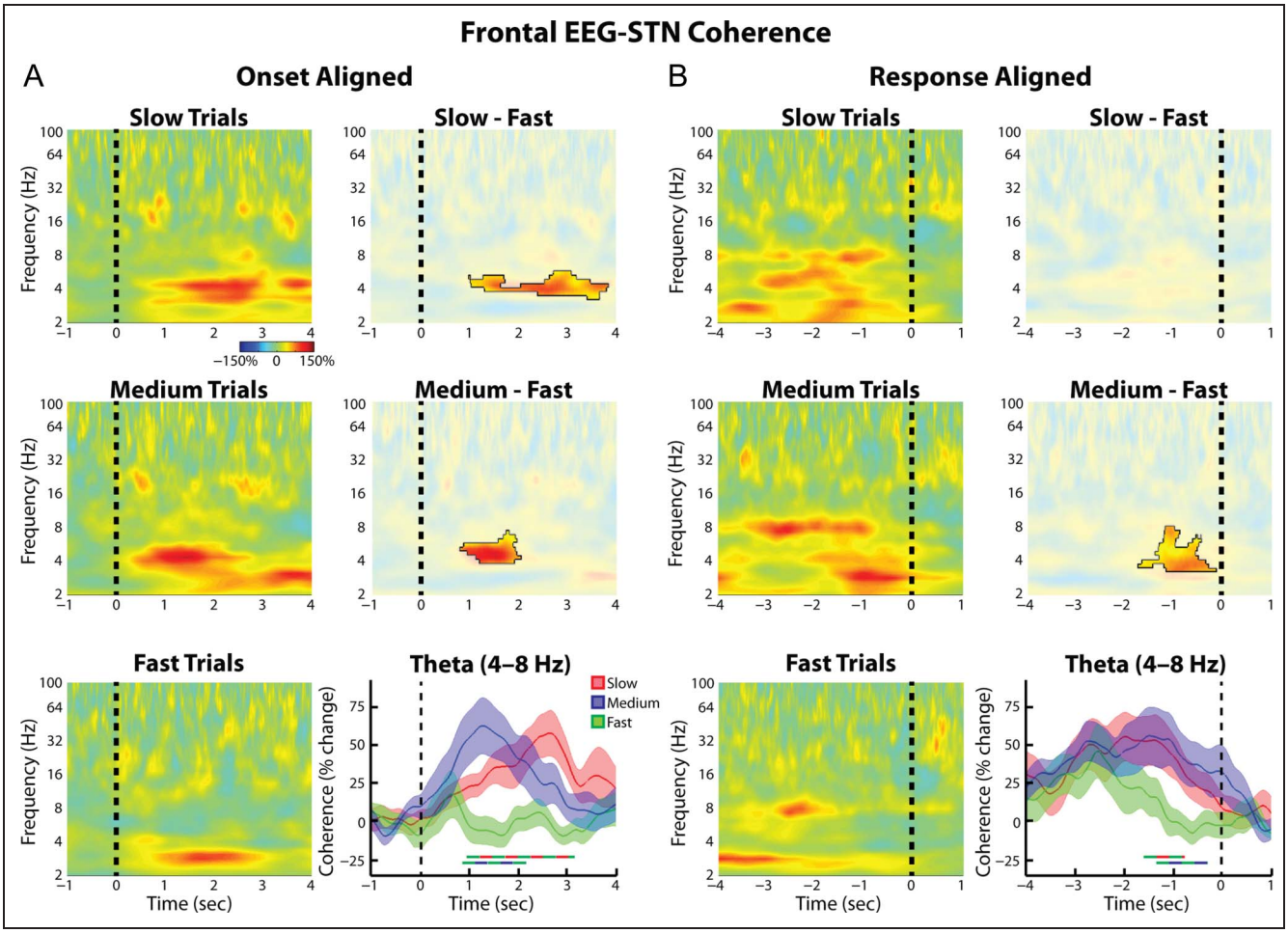

Figure 4. Group average normalized changes in (frontal EEG)–STN LFP wavelet coherence. (A, left) Coherence spectrogram for the slow (top), medium (middle), and fast (bottom) trials. Changes were found relative to a 1-sec long time period between trials during which all dots moved randomly in any direction. (A, right). Differences between slow and fast trials were significant (top, $p = .023$, permutation testing, unmasked area) as were those between the medium and the fast trials (middle, $p = .031$). Time series of percent change in theta band (4–8 Hz) coherence are also shown (bottom, mean ± *SEM*), with thick lines denoting significant time points between two trial types (color of line indicates which two trial types were compared, $p = .003$ for slow vs. fast comparison, $p = .004$ for medium vs. fast comparison, permutation testing). (B) Same as A but for response aligned data. (B, bottom right) Both slow and medium trials showed significantly higher theta coherence in the second preceding the response ($p = .039$ for slow vs. fast comparison, $p = .009$ for medium vs. fast comparison, permutation testing).

medium trials became significantly greater than that observed during the fast trials. During the time point centered 1 sec prior to the response, both medium and slow trials demonstrated coherence values that were significantly greater than baseline ($p = .010$ and $p = .013$, respectively, one sample t test), but the fast trials did not ($p > .95$, one-sample t test). A one-way repeated-measures ANOVA between trial types during this time period revealed a significant effect of Trial type ($F = 6.16$, $df = 2$, $p = .006$). When the individual time points were considered, coherence values in slow trials were found to be significantly greater than in fast trials from −1.60 to −0.77 sec, and those in medium trials were found to be significantly greater from −1.34 to −0.30 sec ($p = .039$ and $p = .009$, respectively, permutation testing). Notably, these differences disappeared by the time the response was executed, further arguing against a time on task interpretation in which the theta coherence would be expected to continue rising until the end of the response.

When the (Pz-Cz)–STN coherence was analyzed, similar trends as those seen for the FCz-Cz–STN connectivity were observed (Figure 5). Although no differences in the (Pz-Cz)–STN coherence multiple comparisons survived correction at the spectrogram level, restricting the analysis to the theta band did reveal some time points that showed significantly higher coherence values during the slow and medium trials relative to the fast trials (Figure 5A). When the time period centered 1 sec prior to the response was considered, a significant effect of Trial type was observed (ANOVA, within-subject repeated-measures, $F = 3.74$, $df = 2$, $p = .04$). In line with this, when we directly tested for an effect of Cortical electrode and Trial type, we did not observe a significant interaction between the two factors (ANOVA, within-subject repeated

measures, Trial type × EEG electrode: Trial type, $F = 5.91$, $df = 2$, $p = .008$; EEG electrode, $F = 0$, $df = 2$, $p = .96$; interaction $F = 2.29$, $df = 2$, $p = .12$).

To test whether the trial-dependent differences in cortical STN theta connectivity were symmetrical or biased in one direction, we repeated the synchrony analysis using Granger causality analytical techniques. When we analyzed the spectral Granger causality in the frontal cortex–STN direction, we also observed significantly high synchrony during the slow and medium trials relative to the fast trials ($p = .021$ and $p = .047$ for the cue aligned slow vs. fast and medium vs. fast comparisons, respectively; Figure 6A). In contrast, the STN–cortex spectral Granger causality did not reveal any significant differences between trial types (Figure 6B). Together these results suggest that the coherence differences reported in the preceding paragraph likely reflect cortex–STN inputs. When we repeated the Granger causality analysis for the posterior cortex recordings (Pz-Cz), we did not reveal any significant differences in cortex–STN and STN–cortex spectral Granger causality (Figure 7). In accordance with the wavelet coherence results, however, when we directly tested for an effect of cortical electrode and trial type, we did not observe a significant interaction between the two factors (ANOVA, within-subject repeated measures, Trial type × EEG electrode: Trial type $F = 2.78$, $df = 2$, $p = .08$; EEG electrode $F = 1.34$, $df = 2$, $p = .27$; interaction $F = 1.54$, $df = 2$, $p = .23$).

DISCUSSION

Previous studies have demonstrated that tasks involving high levels of conflict are associated with increased theta band activity in the mPFC and in the STN (Zavala, Damera, et al., 2015; Cohen & van Gaal, 2014; Zavala et al., 2013, 2014; Brittain et al., 2012; Cavanagh et al., 2011, 2012; Cohen & Cavanagh, 2011). Our previous work using a related paradigm showed that, when a similar number of dots were moving in conflicting directions, theta band activity of the STN became synchronized to that of the mPFC (Zavala et al., 2014). But are such dynamic changes

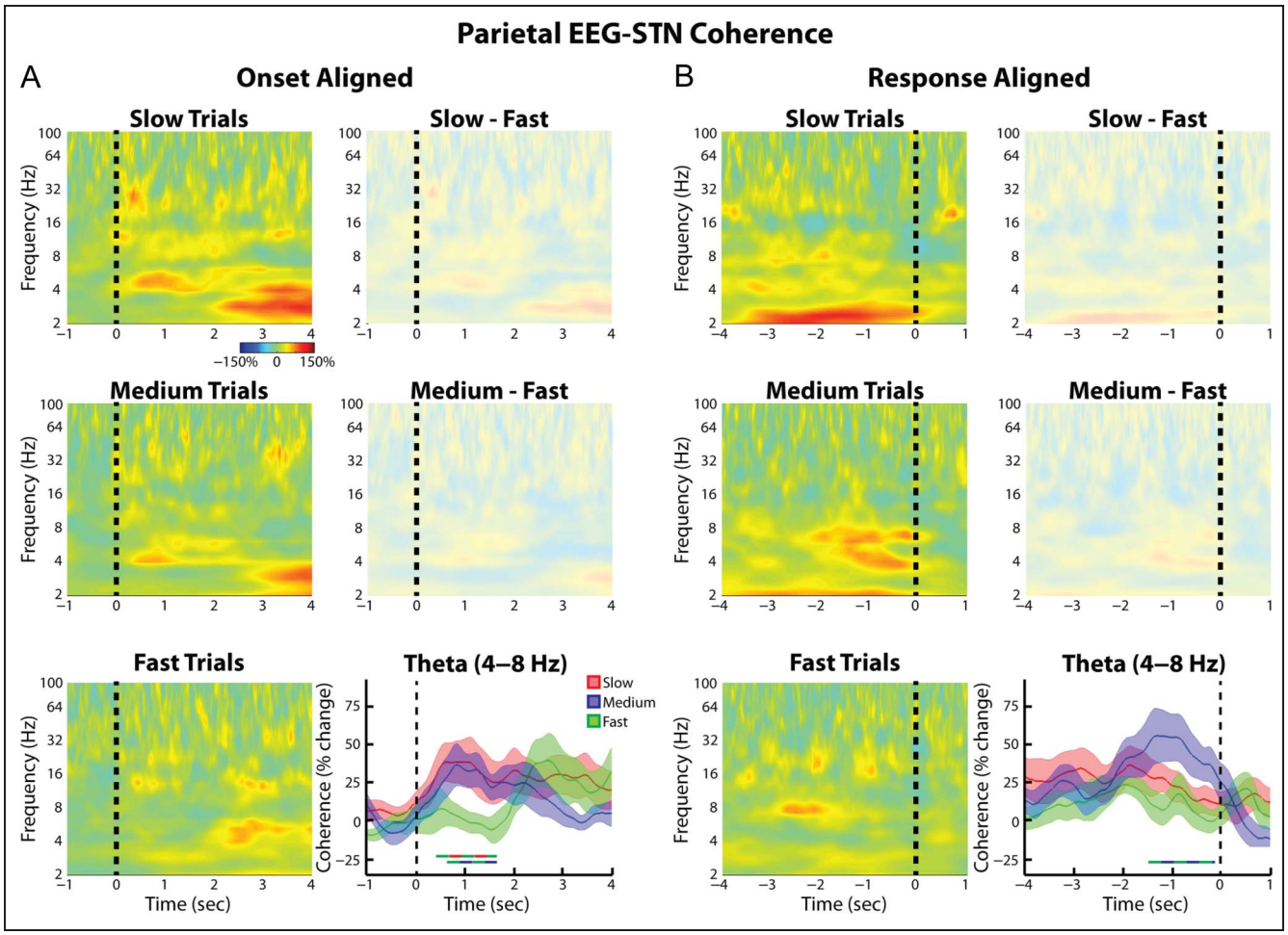

Figure 5. Group average normalized changes in (parietal EEG)–STN LFP wavelet coherence. Same as Figure 4, but for Pz-Cz electrode. Although no significant differences across the whole spectrogram were observed, when the analysis was restricted to the theta band, both the slow and medium trials showed significantly higher theta band phase synchrony relative to the fast trials ($p = .012$ and .033, respectively, permutation testing).

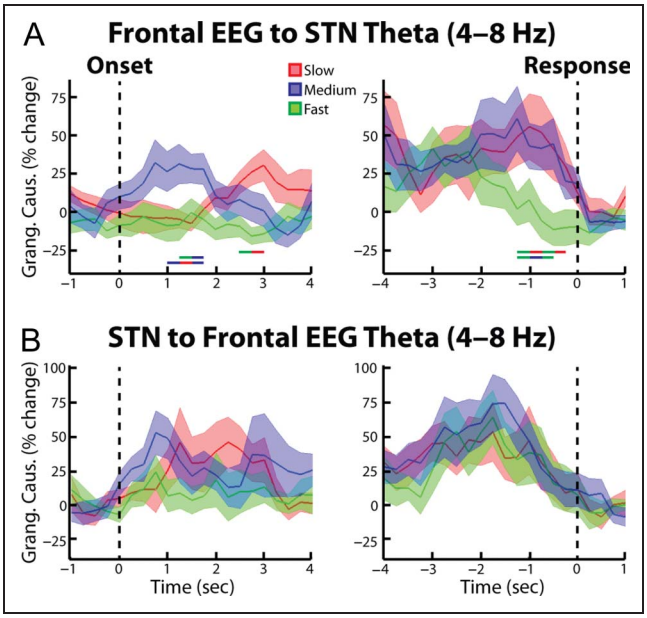

Figure 6. Group average percent change in theta band (4–8 Hz) spectral Granger causality between frontal EEG and STN LFP. (A) EEG–STN spectral Granger causality (mean ± *SEM*) aligned to the congruent dot motion onset (left). Changes were found relative to a 1-sec long time period between trials during which all dots moved randomly in any direction. Thick lines denoting significant time points between two trial types are shown (color of line indicates which two trial types were compared, $p = .021$ for slow vs. fast comparison, $p = .047$ for medium vs. fast comparison, $p = .020$ for slow vs. medium comparison, permutation testing). (A, right) Same as (A, left) but for data aligned to the response ($p = .014$ for slow vs. fast comparison, $p = .009$ for medium vs. fast comparison, permutation testing. (B) Same as A, but for the STN–frontal EEG direction. No significant differences were observed.

in functional connectivity related to conflict per se, or the increased need for cognitive control in difficult tasks?

The novel dot motion discrimination task we used here, in which the rate at which randomly moving dots became congruent was set to three different speeds, allowed us to investigate the mechanisms the brain uses to make sensorimotor decisions in which evidence is incrementally presented. Our results suggest that cortical STN theta synchrony is not only involved in inhibiting responses when stimuli simultaneously activate two or more conflicting motor commands but also when individuals are asked to make decisions during higher levels of uncertainty. The time course of the theta band coherence during the medium and slow trials indicated that, as early as 1.5 sec before the response, cortico-STN networks became synchronized. This suggests that the participants, either consciously or subconsciously (O'Connell et al., 2012), became aware of the congruent dot motion this early, but it took up to an additional 1.5 sec to gather enough evidence to confidently make their decision. We posit that, during this time period, increased synchrony between the cortex and the STN acts to prevent the participants from making a response, paralleling the "hold your horses" role the STN is thought to play during time periods of conflict (Frank et al., 2007). Once other brain structures had integrated enough evidence to make a decision, cortico-STN coherence returned to baseline levels and the movement was processed and executed.

What is the evidence that our three experimental conditions engendered different levels of cognitive control? A priori, one might have expected that there would be a specific threshold of dot congruency below which participants would not be able to perceive congruent dot motion and above which the participants would know with a high degree of certainty the direction in which the dots were moving. If this were the case, all three trial types would have required identical dot congruency at the time of the response. However, instead, during the slowest trials, participants were able to make decisions with less evidence on the screen. This suggests that participants may have integrated dot motion congruency evidence over time until the integral exceeded the same threshold of integrated evidence for fast, medium, and slow trial types. With respect to task uncertainty, the critical feature though is that the level of dot motion congruency up to and including the time of the response was less for medium and slow trials than that for fast trials. We believe that the higher level of ambiguity during slow and medium trials (responses were made with an average of 24% and 33% dot congruency, respectively) could potentially require a higher level of cognitive control than that required during the fast trials (44% average dot congruency at the time of the response). We propose that for this reason we observed elevated theta band

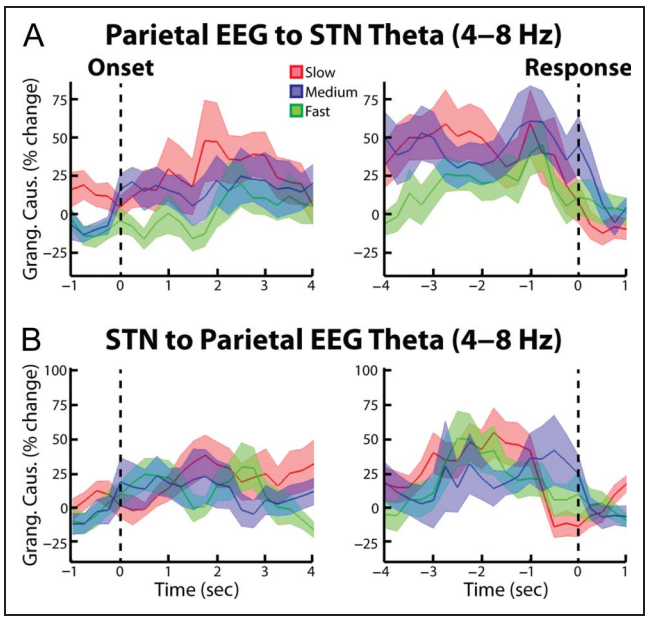

Figure 7. Group average percent change in theta band (4–8 Hz) spectral Granger causality between parietal EEG and STN LFP. Same as Figure 6, but for Pz-Cz electrode. No significant differences were observed ($p > .05$, permutation testing).

coherence between activities in medial EEG electrodes and the STN during the slow and medium trials.

Intriguingly, unlike our previous results involving explicit stimulus conflict (Zavala et al., 2013, 2014), the differences in cortico-STN theta coherence took place without any trial type-related differences in power or ITPC. When we analyzed the average changes in power across all trials, the only change from baseline that we observed was the classic, movement-related beta band power decrease. We also observed a significant delta band ITPC increase in the STN and in the medial frontal EEG electrodes that was similar to that observed in our previous work involving both gradual dot congruency increases (Zavala et al., 2014) and discrete stimuli presentations (Zavala et al., 2013). Taken together, the relative timing of the cortico-STN theta coherence differences between trials and the response-related changes in beta power and delta ITPC changes across all trials suggests that theta band activity may play a role in inhibiting movement whereas beta band suppression and delta band ITPC may be involved in facilitating movement. As we and others have previously argued (Kelly & O'Connell, 2013, 2015; Zavala et al., 2014; O'Connell et al., 2012), the intentional use of gradually evolving continuous stimuli, as opposed to discretely presented stimuli, allows us to separate movement and stimulus-related activity from activity related to the decision-making process.

This study has several possible limitations that should be considered. First, all recordings were made in patients with PD, which has been consistently shown to involve abnormal STN activity (reviewed in Hammond, Bergman, & Brown, 2007). However, all recordings were made with patients on their dopaminergic medication in an attempt to approximate physiological functioning as closely as possible. Second, LFP and EEG recordings can be subject to volume conduction of electrical signals. To mitigate this effect, only bipolar signals were analyzed. Nevertheless, volume conduction does diminish the spatial resolution of our results and may have contributed to why we did not observe significant trial type-by-electrode interactions when we compared (FCz-Cz)–STN coupling to (Pz-Cz)–STN coupling. Although cortical oscillations are thought to be related to structures in the frontal cortex (Womelsdorf, Johnston, et al., 2010; Womelsdorf, Vinck, et al., 2010; Tsujimoto et al., 2006; Wang et al., 2005; Gevins et al., 1997), our data do not allow us to rule out the possibility that other more posterior cortical areas may also be involved. Third, we should acknowledge the effects of any eye movements potentially not rejected through visual inspection of the raw data, particularly as the spectral changes of interest were at low frequencies. Finally, it should be noted that there are several possible alternative interpretations of the results we have presented. For instance, it could be argued that there is still a decision to be made between which direction to take and that there was dot movement in both directions (albeit just stochastic in one) presenting conflict even in the current paradigm. At any given time, instantaneous dot motion congruency was less in the medium and slow trials affording the greatest conflict with the stochastic movement. Accordingly, it might be argued that conflict was present and greater in the medium and slow trials. However, this interpretation would not explain why participants made choices at points with different levels of instantaneous dot motion congruency in the different trial types. The alternative hypothesis, that dot motion congruency is integrated, accounts for this feature and yet means that trials did not differ with respect to the level of explicit conflict at the time of response selection. However, conflict induced need for delay could be reconciled with responses being made at different levels of instantaneous dot motion congruency if task behavior were governed by time-on-task, either because some sort of temporal discounting was at play or the participants were impulsive. In this case, the increasing cost of delaying a response might mean that participants acted despite having resolved less conflict in medium and slow trials. But against this, the error rate was no different between trials, again consistent with the interpretation that participants acted on integrated evidence, which was similar at the time of decision.

Taken together, our data support the idea that enhanced theta synchrony between the STN and midline electrodes may increase the net antikinetic action of the STN. This, however, may be a general operational principle when choosing what to do and precisely when to do it is difficult, regardless of whether this is due to the simultaneous activation of conflicting actions or due to sensory uncertainty. Accordingly, the results presented here provide further insights into the processes that mitigate response inhibition (Bastin et al., 2014; Benis et al., 2014; Alegre et al., 2013; Brittain et al., 2012; Ray et al., 2012; Kühn et al., 2004) and more "higher-level" decisions (Zaghloul et al., 2012; Cavanagh et al., 2011; Fumagalli et al., 2011), as well as help us understand some of the impulsivity related deficits associated with neuropathology (Rustamov et al., 2013; Van Meel, Heslenfeld, Oosterlaan, & Sergeant, 2007; Fitzgerald et al., 2005), dopaminergic medication (Coulthard et al., 2012; Rodriguez-Oroz et al., 2011), and DBS (Antoniades et al., 2014; Hälbig et al., 2009; Frank et al., 2007; Frank, 2006).

Acknowledgments

B. Z. is supported by the Rhodes Trust and the National Institutes of Health Oxford-Cambridge fellowship. M. H., T. F., and L. Z. are funded by the Department of Health, National Institute for Health Research, University College London Biomedical Research Center; The Monument Trust; and Parkinson's Appeal for Deep Brain Stimulation. P. B. and H. T. are funded by the Medical Research Council, and P. B. is further funded by the Department of Health, National Institute for Health Research, Oxford Biomedical Research Centre. S. L. is funded by the Wellcome Trust. This work was partly carried out in the National Institute for Health Research cognitive health Clinical Research Facility, Oxford.

Reprint requests should be sent to Professor Peter Brown, Nuffield Department of Clinical Neurology, University of Oxford, Level 6, West Wing, John Radcliffe Hospital, Oxford, OX3 9DU, UK, or via e-mail: peter.brown@ndcn.ox.ac.uk.

REFERENCES

Alegre, M., Lopez-Azcarate, J., Obeso, I., Wilkinson, L., Rodriguez-Oroz, M. C., Valencia, M., et al. (2013). The subthalamic nucleus is involved in successful inhibition in the stop-signal task: A local field potential study in Parkinson's disease. *Experimental Neurology, 239,* 1–12.

Antoniades, C. A., Bogacz, R., Kennard, C., FitzGerald, J. J., Aziz, T., & Green, A. L. (2014). Deep brain stimulation abolishes slowing of reactions to unlikely stimuli. *Journal of Neuroscience, 34,* 10844–10852.

Bastin, J., Polosan, M., Benis, D., Goetz, L., Bhattacharjee, M., Piallat, B., et al. (2014). Inhibitory control and error monitoring by human subthalamic neurons. *Translational Psychiatry, 4,* e439.

Benis, D., David, O., Lachaux, J.-P., Seigneuret, E., Krack, P., Fraix, V., et al. (2014). Subthalamic nucleus activity dissociates proactive and reactive inhibition in patients with Parkinson's disease. *Neuroimage, 91,* 273–281.

Bogacz, R., & Gurney, K. (2007). The basal ganglia and cortex implement optimal decision making between alternative actions. *Neural Computation, 19,* 442–477.

Botvinick, M. M., Cohen, J. D., & Carter, C. S. (2004). Conflict monitoring and anterior cingulate cortex: An update. *Trends in Cognitive Sciences, 8,* 539–546.

Brittain, J.-S., Watkins, K. E., Joundi, R. A., Ray, N. J., Holland, P., Green, A. L., et al. (2012). A role for the subthalamic nucleus in response inhibition during conflict. *Journal of Neuroscience, 32,* 13396–13401.

Brovelli, A., Ding, M., Ledberg, A., Chen, Y., Nakamura, R., & Bressler, S. L. (2004). Beta oscillations in a large-scale sensorimotor cortical network: Directional influences revealed by Granger causality. *Proceedings of the National Academy of Sciences, U.S.A., 101,* 9849–9854.

Cavanagh, J. F., & Shackman, A. J. (2015). Frontal midline theta reflects anxiety and cognitive control: Meta-analytic evidence. *Journal of Physiology (Paris), 109,* 3–15.

Cavanagh, J. F., Wiecki, T. V., Cohen, M. X., Figueroa, C. M., Samanta, J., Sherman, S. J., et al. (2011). Subthalamic nucleus stimulation reverses mediofrontal influence over decision threshold. *Nature Neuroscience, 14,* 1462–1467.

Cavanagh, J. F., Zambrano-Vazquez, L., & Allen, J. J. B. (2012). Theta lingua franca: A common midfrontal substrate for action monitoring processes. *Psychophysiology, 49,* 220–238.

Cohen, M. X. (2014). *Analyzing neural time series data: Theory and practice*. Cambridge, MA: MIT Press.

Cohen, M. X., & Cavanagh, J. F. (2011). Single-trial regression elucidates the role of prefrontal theta oscillations in response conflict. *Frontiers in Perception Science, 2,* 30.

Cohen, M. X., & Gulbinaite, R. (2014). Five methodological challenges in cognitive electrophysiology. *Neuroimage, 85,* 702–710.

Cohen, M. X., & Nigbur, R. (2013). Reply to "Higher response time increases theta energy, conflict increases response time." *Clinical Neurophysiology, 124,* 1479–1481.

Cohen, M. X., & van Gaal, S. (2014). Subthreshold muscle twitches dissociate oscillatory neural signatures of conflicts from errors. *Neuroimage, 86,* 503–513.

Coulthard, E. J., Bogacz, R., Javed, S., Mooney, L. K., Murphy, G., Keeley, S., et al. (2012). Distinct roles of dopamine and subthalamic nucleus in learning and probabilistic decision making. *Brain, 135,* 3721–3734.

Ding, M., Bressler, S. L., Yang, W., & Liang, H. (2000). Short-window spectral analysis of cortical event-related potentials by adaptive multivariate autoregressive modeling: Data preprocessing, model validation, and variability assessment. *Biological Cybernetics, 83,* 35–45.

Ding, M., Chen, Y., & Bressler, S. L. (2006). Granger causality: Basis theory and application to neuroscience. In B. Schelter, M. Winterhalder, & J. Timmer (Eds.), *Handbook of time series analysis: Recent theoretical developments and applications* (pp. 437–460). Berlin: Wiley-VCH. Available at: www.ccs.fau.edu/~bressler/pdf/HTSA06.pdf.

Fitzgerald, K. D., Welsh, R. C., Gehring, W. J., Abelson, J. L., Himle, J. A., Liberzon, I., et al. (2005). Error-related hyperactivity of the anterior cingulate cortex in obsessive-compulsive disorder. *Biological Psychiatry, 57,* 287–294.

Foltynie, T., & Hariz, M. I. (2010). Surgical management of Parkinson's disease. *Expert Review of Neurotherapeutics, 10,* 903–914.

Frank, M. J. (2006). Hold your horses: A dynamic computational role for the subthalamic nucleus in decision making. *Neural Networks, 19,* 1120–1136.

Frank, M. J., Samanta, J., Moustafa, A. A., & Sherman, S. J. (2007). Hold your horses: Impulsivity, deep brain stimulation, and medication in parkinsonism. *Science, 318,* 1309–1312.

Fumagalli, M., Giannicola, G., Rosa, M., Marceglia, S., Lucchiari, C., Mrakic-Sposta, S., et al. (2011). Conflict-dependent dynamic of subthalamic nucleus oscillations during moral decisions. *Social Neuroscience, 6,* 243–256.

Gardner, W. A. (1992). A unifying view of coherence in signal processing. *Signal Processing, 29,* 113–140.

Gevins, A., Smith, M. E., McEvoy, L., & Yu, D. (1997). High-resolution EEG mapping of cortical activation related to working memory: Effects of task difficulty, type of processing, and practice. *Cerebral Cortex, 7,* 374–385.

Geweke, J. (1982). Measurement of linear dependence and feedback between multiple time series. *Journal of the American Statistical Association, 77,* 304–313.

Granger, C. (1969). Investigating causal relations by econometric models and cross-spectral methods. *Econometrica, 37,* 424–438.

Green, N., Bogacz, R., Huebl, J., Beyer, A.-K., Kühn, A. A., & Heekeren, H. R. (2013). Reduction of influence of task difficulty on perceptual decision making by STN deep brain stimulation. *Current Biology, 23,* 1681–1684.

Hälbig, T. D., Tse, W., Frisina, P. G., Hollander, E., Shapiro, H., Tagliati, M., et al. (2009). Subthalamic deep brain stimulation and impulse control in Parkinson's disease. *European Journal of Neurology, 16,* 493–497.

Hammond, C., Bergman, H., & Brown, P. (2007). Pathological synchronization in Parkinson's disease: Networks, models and treatments. *Trends in Neurosciences, 30,* 357–364.

Kamiński, M. J., & Blinowska, K. J. (1991). A new method of the description of the information flow in the brain structures. *Biological Cybernetics, 65,* 203–210.

Kelly, S. P., & O'Connell, R. G. (2013). Internal and external influences on the rate of sensory evidence accumulation in the human brain. *Journal of Neuroscience, 33,* 19434–19441.

Kelly, S. P., & O'Connell, R. G. (2015). The neural processes underlying perceptual decision making in humans: Recent progress and future directions. *Journal of Physiology (Paris), 109,* 27–37.

Krain, A. L., Wilson, A. M., Arbuckle, R., Castellanos, F. X., & Milham, M. P. (2006). Distinct neural mechanisms of risk and ambiguity: A meta-analysis of decision-making. *Neuroimage, 32,* 477–484.

Kühn, A. A., Williams, D., Kupsch, A., Limousin, P., Hariz, M., Schneider, G.-H., et al. (2004). Event-related beta

desynchronization in human subthalamic nucleus correlates with motor performance. *Brain, 127,* 735–746.
Lachaux, J.-P., Lutz, A., Rudrauf, D., Cosmelli, D., Le Van Quyen, M., Martinerie, J., et al. (2002). Estimating the time-course of coherence between single-trial brain signals: An introduction to wavelet coherence. *Clinical Neurophysiology, 32,* 157–174.
Maris, E., & Oostenveld, R. (2007). Nonparametric statistical testing of EEG- and MEG-data. *Journal of Neuroscience Methods, 164,* 177–190.
Mushtaq, F., Bland, A. R., & Schaefer, A. (2011). Uncertainty and cognitive control. *Frontiers in Psychology, 2,* 249.
Nachev, P. (2011). The blind executive. *Neuroimage, 57,* 312–313.
O'Connell, R. G., Dockree, P. M., & Kelly, S. P. (2012). A supramodal accumulation-to-bound signal that determines perceptual decisions in humans. *Nature Neuroscience, 15,* 1729–1735.
Peirce, J. W. (2007). PsychoPy—Psychophysics software in Python. *Journal of Neuroscience Methods, 162,* 8–13.
Pesaran, B. (2008). Short course III, presented at 2008 Society for Neuroscience Annual Meeting. In P. Mitra (Ed.), *Neural signal processing: Quantitative analysis of neural activity*. Washington, DC: Society for Neuroscience.
Ratcliff, R., & Frank, M. J. (2012). Reinforcement-based decision making in corticostriatal circuits: Mutual constraints by neurocomputational and diffusion models. *Neural Computation, 24,* 1186–1229.
Ratcliff, R., & McKoon, G. (2008). The diffusion decision model: Theory and data for two-choice decision tasks. *Neural Computation, 20,* 873–922.
Ratcliff, R., & Tuerlinckx, F. (2002). Estimating parameters of the diffusion model: Approaches to dealing with contaminant reaction times and parameter variability. *Psychonomic Bulletin & Review, 9,* 438–481.
Ray, N. J., Brittain, J.-S., Holland, P., Joundi, R. A., Stein, J. F., Aziz, T. Z., et al. (2012). The role of the subthalamic nucleus in response inhibition: Evidence from local field potential recordings in the human subthalamic nucleus. *Neuroimage, 60,* 271–278.
Rodriguez-Oroz, M. C., López-Azcárate, J., Garcia-Garcia, D., Alegre, M., Toledo, J., Valencia, M., et al. (2011). Involvement of the subthalamic nucleus in impulse control disorders associated with Parkinson's disease. *Brain, 134,* 36–49.
Ruiz, M. H., Huebl, J., Schönecker, T., Kupsch, A., Yarrow, K., Krauss, J. K., et al. (2014). Involvement of human internal globus pallidus in the early modulation of cortical error-related activity. *Cerebral Cortex, 24,* 1502–1517.
Rustamov, N., Rodriguez-Raecke, R., Timm, L., Agrawal, D., Dressler, D., Schrader, C., et al. (2013). Absence of congruency sequence effects reveals neurocognitive inflexibility in Parkinson's disease. *Neuropsychologia, 51,* 2976–2987.
Scherbaum, S., & Dshemuchadse, M. (2013). Higher response time increases theta energy, conflict increases response time. *Clinical Neurophysiology, 124,* 1477–1479.
Schlögl, A., & Supp, G. (2006). Analyzing event-related EEG data with multivariate autoregressive parameters. *Progress in Brain Research, 159,* 135–147.
Seth, A. K. (2010). A MATLAB toolbox for Granger causal connectivity analysis. *Journal of Neuroscience Methods, 186,* 262–273.
Stern, E. R., Gonzalez, R., Welsh, R. C., & Taylor, S. F. (2010). Updating beliefs for a decision: Neural correlates of uncertainty and underconfidence. *Journal of Neuroscience, 30,* 8032–8041.
Tsujimoto, T., Shimazu, H., & Isomura, Y. (2006). Direct recording of theta oscillations in primate prefrontal and anterior cingulate cortices. *Journal of Neurophysiology, 95,* 2987–3000.
Van Meel, C. S., Heslenfeld, D. J., Oosterlaan, J., & Sergeant, J. A. (2007). Adaptive control deficits in attention-deficit/hyperactivity disorder (ADHD): The role of error processing. *Psychiatry Research, 151,* 211–220.
Wang, C., Ulbert, I., Schomer, D. L., Marinkovic, K., & Halgren, E. (2005). Responses of human anterior cingulate cortex microdomains to error detection, conflict monitoring, stimulus-response mapping, familiarity, and orienting. *Journal of Neuroscience, 25,* 604–613.
White, T. P., Engen, N. H., Sørensen, S., Overgaard, M., & Shergill, S. S. (2014). Uncertainty and confidence from the triple-network perspective: Voxel-based meta-analyses. *Brain and Cognition, 85,* 191–200.
Womelsdorf, T., Johnston, K., Vinck, M., & Everling, S. (2010). Theta-activity in anterior cingulate cortex predicts task rules and their adjustments following errors. *Proceedings of the National Academy of Sciences, U.S.A., 107,* 5248–5253.
Womelsdorf, T., Vinck, M., Leung, L. S., & Everling, S. (2010). Selective theta-synchronization of choice-relevant information subserves goal-directed behavior. *Frontiers in Human Neuroscience, 4,* 210.
Yeung, N., Cohen, J. D., & Botvinick, M. M. (2011). Errors of interpretation and modeling: A reply to Grinband et al. *Neuroimage, 57,* 316–319.
Zaghloul, K. A., Weidemann, C. T., Lega, B. C., Jaggi, J. L., Baltuch, G. H., & Kahana, M. J. (2012). Neuronal activity in the human subthalamic nucleus encodes decision conflict during action selection. *Journal of Neuroscience, 32,* 2453–2460.
Zavala, B., Brittain, J.-S., Jenkinson, N., Ashkan, K., Foltynie, T., Limousin, P., et al. (2013). Subthalamic nucleus local field potential activity during the Eriksen flanker task reveals a novel role for theta phase during conflict monitoring. *Journal of Neuroscience, 33,* 14758–14766.
Zavala, B., Damera, S., Dong, J. W., Lungu, C., Brown, P., & Zaghloul, K. A. (2015). Human subthalamic nucleus theta and beta oscillations entrain neuronal firing during sensorimotor conflict. *Cerebral Cortex,* bhv244.
Zavala, B., Zaghloul, K., & Brown, P. (2015). The subthalamic nucleus, oscillations, and conflict. *Movement Disorders, 30,* 328–338.
Zavala, B. A., Tan, H., Little, S., Ashkan, K., Hariz, M., Foltynie, T., et al. (2014). Midline frontal cortex low-frequency activity drives subthalamic nucleus oscillations during conflict. *Journal of Neuroscience, 34,* 7322–7333.